Sustainable Energy & Fuels

Nitrogen/fluorine-codoped rutile titania as a stable oxygen-evolution photocatalyst for solar-driven Z-scheme water splitting

Journal:	*Sustainable Energy & Fuels*
Manuscript ID	SE-ART-04-2018-000191.R1
Article Type:	Paper
Date Submitted by the Author:	08-May-2018

Complete List of Authors:	Miyoshi, Akinobu; Tokyo Institute of Technology, Chemitry Vequizo, Junie Jhon; Toyota Technological Institute, Graduate School of Engineering Nishioka, Shunta; Tokyo Institute of Technology, Chemistry Kato, Yuma; Osaka City University Yamamoto, Muneaki; Nagoya university, Graduate School of Engineering Yamashita, Shunsuke; National Institute for Materials Science Yokoi, Toshiyuki; Tokyo Institute of Technology, Institute of Innovative Research Iwase, Akihide; Tokyo University of Science, Nozawa, Shunsuke; High Energy Accelerator Research Organization, Photon Factory Yamakata, Akira; Toyota Technological Institute, Graduate School of Enginnering Yoshida, Tomoko; Osaka City University, Kimoto, Koji; National Institute for Materials Science, Kudo, Akihiko; Tokyo University of Science, Maeda, Kazuhiko ; Tokyo Institute of Technology, Chemistry

Journal Name

ARTICLE

Nitrogen/fluorine-codoped rutile titania as a stable oxygen-evolution photocatalyst for solar-driven Z-scheme water splitting†

Received 00th January 20xx,
Accepted 00th January 20xx

DOI: 10.1039/x0xx00000x

www.rsc.org/

Akinobu Miyoshi,[a] Junie Jhon M. Vequizo,[b] Shunta Nishioka,[a,c] Yuma Kato,[d] Muneaki Yamamoto,[e] Shunsuke Yamashita,[f] Toshiyuki Yokoi,[g] Akihide Iwase,[h,i] Shunsuke Nozawa,[j] Akira Yamakata,[b] Tomoko Yoshida,[d] Koji Kimoto,[f] Akihiko Kudo,[h,i] and Kazuhiko Maeda*[a]

Nitrogen/fluorine-codoped rutile TiO_2 (R-TiO_2:N,F) was newly synthesized, and its photocatalytic activity for water oxidation was evaluated. R-TiO_2:N,F could be prepared by nitridation of rutile TiO_2 (R-TiO_2) and $(NH_4)_2TiF_6$ mixture at 773 K. The prepared samples produced O_2 from aqueous $AgNO_3$ solution under visible light irradiation, while R-TiO_2 nitrided at the same temperature without fluorine source showed negligible activity. The highest activity was obtained with the sample prepared at the $(NH_4)_2TiF_6$/R-TiO_2 ratio of 15/85, exhibiting water oxidation activity even in the presence of a reversible electron acceptor such as IO_3^- or Fe^{3+} with the aid of RuO_2 cocatalyst. Stoichiometric water splitting into H_2 and O_2 evolution was achieved using a mixture of Ru/$SrTiO_3$:Rh and RuO_2/TiO_2:N,F in the presence of $[Co(bpy)_3]^{3+/2+}$ (bpy = 2,2'-bipyridine) as a shuttle redox mediator without noticeable degradation of activity under visible light and even under AM1.5G simulated sunlight. Transient absorption spectroscopy revealed that appropriate nitrogen/fluorine codoping reduces the density of mid-gap states working as deep traps of photogenerated electrons, and increases number of free electrons compared to only nitrogen-doped R-TiO_2. Experimental results highlighted that photocatalytic activity of the R-TiO_2:N,F could be enhanced by improving visible-light absorption capability through the N/F codoping while suppressing the density of deep trap sites.

Introduction

Exploring a new material that exhibits useful functionality is an important mission in materials chemistry. Of particular interest is the use of p-block elements, which are earth-abundant and light, for synthesizing such a functional material. Mixed anion compounds that contain more than two different anions have recently attracted attention as new class of materials that exhibit interesting properties including superconductivity, dielectric property, catalysis and photocatalysis.[1]

Photocatalytic reactions such as water splitting and CO_2 fixation on illuminated semiconductors have attracted considerable attention from the viewpoint of solar-to-fuel energy conversion.[2–13] For efficient utilization of solar energy, visible-light-responsive photocatalyst is necessary since the visible light constitute a half of the solar spectrum. In this regard, visible-light absorption capability of narrow-gap mixed anion compounds, which is in general difficult to be attained by oxide materials, well fits the bill.[1] For example, oxynitrides have energy levels derived from N 2p state above the O 2p state, causing oxynitrides to have narrower band gaps than corresponding metal oxides.[4,9] Because certain (oxy)nitrides exhibit high photocatalytic activity for water oxidation under visible light,[4] they are potential candidates not only for water splitting but also for CO_2 fixation.[12,13]

However, synthesis of a mixed anion compound that shows high photocatalytic activity is not always easy. One of the reasons for this is the charge compensation issue when substituting an anion for another that has different charges (e.g., O^{2-}/N^{3-} exchange). For example, nitrogen-doped TiO_2 has been intensively studied as a visible-light-responsive photocatalyst since the report by Asahi *et al.*[14] Although various synthetic routes to nitrogen-doped TiO_2 are available,[14–24] the low concentration of nitrogen introduced into TiO_2 lattice limits the visible light absorption capability,

[a] Department of Chemistry, School of Science, Tokyo Institute of Technology, 2-12-1-NE-2 Ookayama, Meguro-ku, Tokyo 152-8550, Japan.
[b] Graduate School of Engineering, Toyota Technological Institute, 2-12-1 Hisakata, Tempaku, Nagoya 468-8511, Japan.
[c] Japan Society for the Promotion of Science, Kojimachi Business Centre Building, 5-3-1, Kojimachi, Chiyoda-ku, Tokyo 102-0083, Japan.
[d] Advanced Research Institute for Natural Science and Technology, Osaka City University, 3-3-138 Sugimoto Sumiyoshi-ku, Osaka, 558-8585, Japan.
[e] Institute of Materials and Systems for Sustainability, Nagoya University, Furo-cho, Chikusa-ku, Nagoya 464-8603, Japan.
[f] Electron Microscopy Group, Research Center for Advanced Measurement and Characterization, National Institute for Materials Science, 1-1 Namiki, Tsukuba 305-0044, Japan.
[g] Nanospace Catalysis Unit, Institute of Innovative Research, Tokyo Institute of Technology, 4259 Nagatsuta, Midori-ku, Yokohama 226-8503, Japan.
[h] Department of Applied Chemistry, Faculty of Science, Tokyo University of Science, 1-3 Kagurazaka, Shinjuku-ku, Tokyo 162-8601, Japan.
[i] Photocatalysis International Research Centre, Research Institute for Science and Technology, Tokyo University of Science, 2641 Noda-shi, Yamazaki, Chiba 278-8510, Japan.
[j] Institute of Materials Structure Science, High Energy Accelerator Research Organization, 1-1 Oho, Tsukuba, Ibaraki 305-0801, Japan.
† Electronic Supplementary Information (ESI) available: [Additional characterization and reaction data]. See DOI: 10.1039/x0xx00000x

resulting in lower photocatalytic activity. More importantly, such "aliovalent" substitution in a metal oxide causes the generation of oxygen vacancies, which contribute to lower photocatalytic activity.[24] Another difficulty in synthesizing a mixed anion compound arises from the metastability relative to the corresponding oxide materials.[1] While synthesis of a new mixed anion compound is very exciting and important, there remains a challenge.

Codoping of two different anions is a potential means of addressing the charge imbalance issue in a doped metal oxide. Domen *et al*. reported that nitrogen/fluorine codoping into anatase TiO_2 resulted in more pronounced visible light absorption and higher photocatalytic activity for water oxidation, compared to nitrogen only doped analogue.[16–18] According to that report, this is primarily attributed to an increase in the nitrogen content because of fluorine compensating the charge imbalance caused by nitrogen. Since then, several groups have reported N/F-codoped TiO_2 not only for water reduction/oxidation but also for environmental purification.[19–21]

In this work, we focused on N/F-codoped rutile TiO_2 (R-TiO_2:N,F). Rutile TiO_2 (Fig. 1), a well-known wide-gap semiconductor applicable to several types of photocatalytic reactions,[25–30] has been reported to possess unique photocatalytic properties for oxygen evolution, which can be beneficial for Z-scheme water splitting.[25,31–34] Therefore, R-TiO_2:N,F is of interest as a potential photocatalyst for water oxidation under visible light. While N/F-codoped anatase TiO_2 has been reported already as mentioned above,[16–21] however, no report is available for the rutile form. This might be at least in part due to the nature of anatase-to-rutile phase transition, which typically occurs at high temperatures.[35,36] High temperature ammonolysis, which is essential for introduction of nitrogen into metal oxides,[1] may cause the generation of other thermally stable phases such as TiN,[37] making it difficult to obtain single-phase rutile structure.

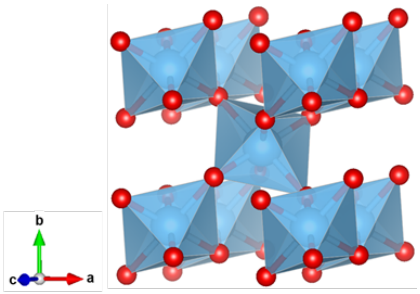

Fig. 1. Crystal structure of rutile TiO_2 (ICSD: 165925).

For the development of a highly efficient semiconductor photocatalyst, it is undoubtedly important to understand photogenerated charge carrier dynamics in a semiconductor. Transient absorption spectroscopy (TAS) is a powerful technique that can visualize the dynamics of electrons and holes generated in an illuminated semiconductor.[24,38–47] In fact, carrier dynamics of binary mixed anion semiconductors such as oxynitrides have been investigated by means of TAS, with several examples available already.[24,43–45] For ternary anion systems such as N/F-codoped oxides, however, such a spectroscopic study had not been done, and there is little information on photogenerated charge carrier dynamics in ternary mixed anion systems. The lack of such spectroscopic information makes it difficult to establish a rational strategy for developing a highly active ternary mixed anion photocatalyst.

Here we report a simple synthetic route to synthesize R-TiO_2:N,F, which is active for photocatalytic water oxidation under visible light even in a non-sacrificial manner with a reversible electron acceptor to achieve Z-scheme water splitting. Photocatalytic activities of the synthesized materials are discussed, on basis of the results of physicochemical analyses and transient absorption spectroscopy measurement, in order to show a rational guideline to synthesize an active R-TiO_2:N,F photocatalyst.

Experimental

Materials and reagents

Rutile TiO_2 (R-TiO_2; 99.0%, Wako Pure Chemicals), $(NH_4)_2TiF_6$ (95.0%, Wako Pure Chemicals), $Sr(OH)_2{\cdot}8H_2O$ (96.0%, Kanto Chemical), anatase TiO_2 (JRC-TIO-10), $Rh(NO_3)_3$ (80.0% as metallic Rh, Kanto Chemical), $RuCl_3{\cdot}nH_2O$ (Ru 41.35 wt%; Furuya Metal), $AgNO_3$ (99.8%; Wako Pure Chemicals), La_2O_3 (99.9%; TCI), $NaIO_3$ (99.5%; Kanto Chemical), $FeCl_3{\cdot}6H_2O$ (99.0%, Kanto Chemical), $CoSO_4{\cdot}7H_2O$ (99.9%; Kanto Chemical), 2,2'-bipyridine (99.0%; Kanto Chemical), methanol (99.8%; Kanto Chemical), acetone (99.5%; Kanto Chemical), I_2 (99.8%; Wako Pure Chemicals) and Na_2SO_4 (99.9%; Wako Pure Chemicals) were used as received.

Synthesis of R-TiO_2:N,F

R-TiO_2:N,F was prepared by nitiridation of R-TiO_2 and $(NH_4)_2TiF_6$ mixture. R-TiO_2 and $(NH_4)_2TiF_6$ were mixed in an agate mortar and a pestle with various molar ratios using an appropriate amount of methanol. The precursor was loaded on a Ni plate and set at the centre of an alumina tube reactor to prevent contamination.[16] After purging air with nitrogen gas, the reactor was heated at 773 K (ramp: 10 K min^{-1}) for 1 h under a dry NH_3 flow (flow rate: 50 mL min^{-1}). For convenience, molar concentration of $(NH_4)_2TiF_6$ in the mixture is represented as *C* in the unit of mol%. *C* = 0 (873 K) samples were synthesized by nitriding R-TiO_2 in the same manner at 873 K without adding $(NH_4)_2TiF_6$.

Synthesis of Rh-doped $SrTiO_3$

The $SrTiO_3$:Rh was obtained by a hydrothermal synthesis according to a previously reported method.[24] In a typical synthesis, 22 mmol of $Sr(OH)_2{\cdot}8H_2O$, 19.6 mmol of TiO_2 (JRC-TIO-10), and 0.5 mmol of $Rh(NO_3)_3$ were mixed in 50 mL of water. The mixture was placed in a Teflon-lined stainless-steel autoclave and heated at 433 K for 42 h. The obtained precipitate washed with hot water and water was dried at 363 K in an oven. The hydrothermal product (0.95 g) was mixed

with an additional amount of $Sr(OH)_2 \cdot 8H_2O$ (95 mg) and heated at 1273 K for 10 h in air. The resulting product was washed with water and dried at 363 K.

Modification of R-TiO_2:N,F with RuO_2 cocatalyst

R-TiO_2:N,F was modified with RuO_2 cocatalyst, which work as both reduction and oxidation sites,[48] by previously reported method.[49] R-TiO_2:N,F was dispersed in $RuCl_3$ aqueous solution containing 0.5 wt% of Ru as to R-TiO_2:N,F for 3 h. The material was collected by filtration and dried at 343 K overnight. The amount of the deposited Ru was 0.3 wt%, which was determined by inductively coupled optical emission spectroscopy (5100 VDV ICP-OES, Agilent Technologies) measured by Ookayama Materials Analysis Division, Technical Department, Tokyo Institute of Technology.

General characterization

X-ray diffraction (XRD) patterns were recorded on a MiniFlex600 (Rigaku) powder diffractometer. Diffuse reflectance spectra (DRS) were obtained using V-670 (JASCO) spectrometer equipped with integration sphere using $BaSO_4$ as a reference. Brunauer-Emmett-Teller (BET) surface areas were measured using BELSORP mini (BEL Japan) at liquid nitrogen temperature (77 K). Surface morphology was observed by a scanning electron microscope (SEM; JSM–IT100LA, Jeol or SU9000, Hitachi) equipped with an energy-dispersive X-ray spectroscopy (EDX) apparatus. Amounts of nitrogen and fluorine were determined using elemental analysis (MICRO CORDER JM10, J-SCIENCE; HSU-20+ICS-1100, Yanaco) by Suzukakedai Materials Analysis Division, Technical Department, Tokyo Institute of Technology. Surface atomic compositions were examined by means of X-ray photoelectron spectroscopy (XPS; ESCA-3400, Shimadzu).

STEM observation

A Titan Cubed microscope (FEI) equipped with spherical aberration correctors (CEOS) was used for taking scanning transmission electron microscopy (STEM) images at an acceleration voltage of 300 kV. The convergence semiangle of the incident probe was 25 mrad, with the incident probe current of 20 pA. The detector collection semiangles were from 77 to 200 mrad for high-angle annular dark-field (HAADF) and 10 to 19 mrad for annular bright-field (ABF) imaging, respectively. The acquired images were processed for noise reduction using a Wiener filter implemented as FiltersPro plug-in (HREM Research) for DigitalMicrograph (Gatan).

XAFS measurements

X-ray absorption fine structure (XAFS) measurements were performed for titanium and nitrogen. Ti-K edge XAFS were taken at the beamline 9A of the Photon Factory (High Energy Accelerator Research Organization, Tsukuba, Japan) under the approval of the Photon Factory Advisory Committee (Proposal No. 2014S2-006). The X-ray energy was varied using a Si (111) double-crystal monochromator. The data were processed using Athena.[50] N-K edge X-ray absorption near edge structure (XANES) spectra of the samples were measured at the BL7U stations of Aichi Synchrotron Radiation Center (Proposal No. 201704061), Japan. Data were recorded at room temperature in total electron yield mode, and the X-ray energy dependence of the N Auger electron yield was monitored. Considering the escape depth of the Auger electrons, the spectra probe the sample from the surface up to a few nanometres in depth.

Electrochemical impedance measurements

R-TiO_2:N,F electrodes were prepared by electrophoretic deposition on a conductive glass modified with a fluorine-doped tin oxide (FTO) layer. During the electrophoretic deposition procedure, a pair of FTO glasses were immersed parallel to each other in dispersions of R-TiO_2:N,F powder (50 mg) in an acetone solution (45 mL) containing I_2 (10 mg) at a distance of 1.8 cm, and connected to a DC power supply (GW Instek PSW 80-13.5). A bias of 50 V was applied between the FTO glasses for 15 s, resulting in photocatalyst-coated FTO glass. The coated area was fixed at 1.5 cm × 3.5 cm. The electrode was dried in vacuum for overnight.

Impedance measurements were conducted using a potentiostat (AMETEK VersaSTAT3) in an aqueous 0.1 M Na_2SO_4 solution using the R-TiO_2:N,F/FTO glass as a working electrode, an Ag/AgCl reference electrode (in saturated KCl aqueous solution) and Pt wire as a counter electrode. The solution was purged with argon for 15 min. The pH of the solution was adjusted by addition of H_2SO_4 or NaOH as needed. Mott-Schottky plots were prepared at a frequency of 100 Hz.

Transient absorption spectroscopy

Measurements were conducted using a homemade spectrometer described previously.[38] R-TiO_2:N,F samples were fixed on a CaF_2 plate at a density of 1.5 mg cm^{-2} and placed into an IR cell for measurements. The samples were photoexcited using 480-nm pulses from an Nd:YAG laser (Continuum Surelite I; duration, 6 ns; power, 0.5 mJ; repetition rate, 5–0.1 Hz), and transient absorptions in the visible to mid-IR region were measured under nitrogen atmosphere. The time resolution of this spectrometer was limited to 1–2 μs by the bandwidth of the amplifier (Stanford Research Systems, SR560, 1 MHz).

Photocatalytic reactions

Photocatalytic reactions were conducted in a Pyrex top-irradiation type reaction vessel connected to closed circulation system. In a reaction vessel, 50 mg of photocatalyst was dispersed in 140 mL of aqueous solution containing 10 mM $AgNO_3$, $NaIO_3$ or $FeCl_3$ that work as electron acceptors. When using $AgNO_3$ solution, 200 mg of La_2O_3 heated at 1273 K for 2 h before use was added as a buffer. The system was evacuated several times to remove air and then, a small amount of Ar gas was introduced prior to irradiation. Light was irradiated through water filter, in combination with a proper cutoff filter and a CM-1 cold mirror. Evolved gases were analysed by an on-line gas chromatograph (GC-8A with TCD detector and MS-5A column, Ar carrier gas, Shimadzu). For the light source, 300 W

Xe lamp was used. The output current was set to 20 A unless otherwise stated. The solution was kept at room temperature by a flow of cooling water during the reaction.

Z-scheme water splitting was conducted in a similar manner. $Ru/SrTiO_3$:Rh (25 mg) and RuO_2/TiO_2:N,F (50 mg) were suspended in an aqueous tris(2,2′-bipyridyl)cobalt(II) sulfate ($[Co(bpy)_3]^{2+}$, 0.5 mM) solution (120 mL). The cobalt complex was synthesized according to the previous method.[51] After removing residual air from the reaction system, irradiation ($420 < \lambda < 800$ nm) was done in the same manner unless otherwise stated.

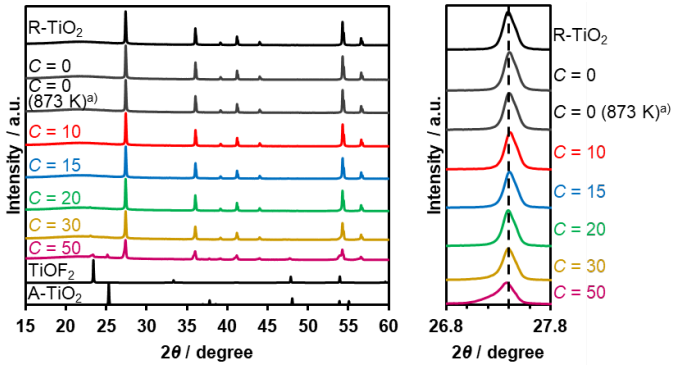

Fig. 2. XRD patterns of R-TiO_2:N,F obtained by nitriding the mixture of R-TiO_2 and $(NH_4)_2TiF_6$ with various concentrations of $(NH_4)_2TiF_6$ at 773 K for 1 h. $TiOF_2$ (ICSD: 38132) and anatase TiO_2 (A-TiO_2) (ICSD: 161908) are shown as reference.

Results and discussion

X-ray diffraction, elemental analyses and electron microscopy

Thermal treatment of a physical mixture of R-TiO_2 and $(NH_4)_2TiF_6$ under a flow of NH_3 gas resulted in the production of orange/yellow powder, depending on the *C* value in the synthesis. XRD patterns of the as-obtained samples are shown in Fig. 2, which indicated that they are mainly consisted of R-TiO_2 structure. More importantly, for samples prepared with higher *C* values (i.e., higher concentration of $(NH_4)_2TiF_6$), diffraction peaks corresponding to R-TiO_2 show shoulders at the lower angles side. This suggests that the occurrence of partial incorporation of anions into the lattice of rutile TiO_2, thereby changing the lattice spacing. This peak shift has been observed in nitrogen/fluorine-codoped anatase TiO_2.[17] Although excess addition of $(NH_4)_2TiF_6$ resulted in the formation of impurity phases, samples prepared with $C \leq 20$ did not show such distinct peaks, so that they are considered to be essentially single-phase rutile. The impurity phases observed at higher *C* samples are presumably anion doped anatase TiO_2- and $TiOF_2$-like species, since they are reported to form during pyrolysis of $(NH_4)_2TiF_6$ in the presence of oxygen source.[16] The fact that lower concentration of $(NH_4)_2TiF_6$ does not show peaks related to impurity phases also suggest that these impurity phases are caused by excess presence of $(NH_4)_2TiF_6$.

To further confirm the presence of nitrogen and fluorine in the synthesized samples, elemental analysis was performed. As listed in Table 1, nitrogen and fluorine are detected for all samples nitrided with $(NH_4)_2TiF_6$ ($C \geq 10$). Furthermore, samples prepared with $(NH_4)_2TiF_6$ showed higher nitrogen concentration compared to the samples prepared without $(NH_4)_2TiF_6$, in which the concentration of nitrogen was below detection limit (<0.1 wt%). This can be explained by the fact that fluorine can compensate the charge imbalance caused by nitrogen.[16,17] Note that nitrogen-doping into anatase TiO_2 generally occurs even at lower temperatures (< 773 K),[17] different from rutile TiO_2 that is more nitridation-resistant. Therefore, the codoping with fluorine was essential to achieve higher nitrogen concentration in rutile TiO_2. We also confirmed by means of XPS that contamination of nickel species in the nitrided product from the nickel plate used in the synthesis was negligibly small (see Table S1).

Table 1. Elemental analysis of R-TiO_2:N,F obtained by nitriding the mixture of precursors with different $(NH_4)_2TiF_6$ concentrations at 773 K.

Entry	*C* / mol%	Amount / wt% N	Amount / wt% F
1	TiO_2	-	-
2	0	n.d.	-
3[a)]	0 (873 K)	n.d.	-
4	10	0.30	0.48
5[b)]	15	0.35	0.63
6	20	0.44	1.15
7	30	0.65	2.03
8	50	1.56	3.53

a) Nitrided at 873 K. b) Experimental errors in N and F amount were within ±0.02.

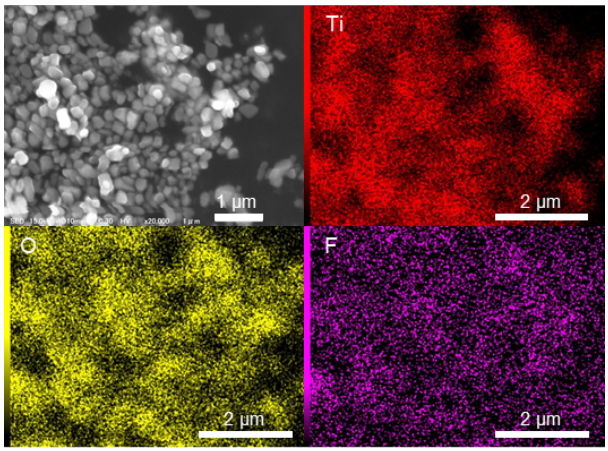

Fig. 3. SEM image and the EDX elemental mapping data of R-TiO_2:N,F (*C* = 15).

Scanning electron microscopy showed that the as-prepared R-TiO_2:N,F samples consisted of 200–300 nm particles, irrespective of *C* value (Figs. 3 and S1). The specific surface areas determined by nitrogen adsorption at 77 K ranged from 5–7 $m^2\ g^{-1}$.

Distribution of nitrogen and fluorine in the R-TiO_2:N,F samples was examined by energy-dispersive X-ray spectroscopy equipped on the SEM apparatus. As shown in Fig. 3, the elemental mapping data indicated that fluorine was uniformly dispersed in the *C* = 15 sample, although the distribution of nitrogen could not be visualized because of the overlap of nitrogen signal with titanium. Similar results were

obtained for C = 10 and 20 samples. For the C = 50 sample, however, fluorine-rich particles were observed, as shown in Fig. S2. The Ti/O/F atomic ratio in the particle was determined to be close to $TiOF_2$, which may support the idea that the impurity observed in XRD (Fig. 2) is $TiOF_2$-like species. Although fluorine-rich particles were observed, other parts of C = 30 and 50 samples showed almost uniform distribution of fluorine. These results suggest that fluorine doping of TiO_2 occurred uniformly in all of the samples, but with some segregation at higher C values.

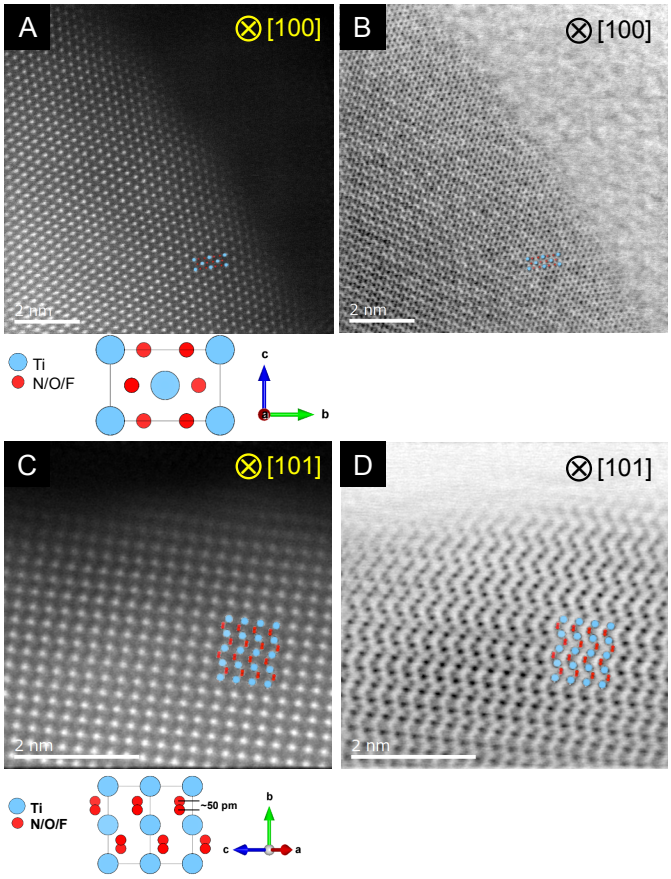

Fig. 4. Results of STEM observations for R-TiO_2:N,F (C = 15). (A, B) HAADF and ABF images taken along [100] and (C, D) [101] direction.

STEM measurements were conducted for the C = 15 sample to obtain atomic-resolution images.[52,53] Fig. 4 shows HAADF and ABF-STEM images. As the signal intensity in HAADF imaging is approximately proportional to Z^2 (where Z represents atomic number),[54] Ti atomic columns in the HAADF images can be seen as bright dots. Here the arrangement of the bright dots agreed well with atomic positions of Ti expected from the crystal structure of rutile TiO_2. It is also noted that the ABF images enabled to visualize the arrangement of anions, which is again consistent with that in the rutile structure. The STEM observations thus confirmed the generation of rutile-type structure of R-TiO_2:N,F (C = 15), in good agreement with the result of XRD analysis (Fig. 2).

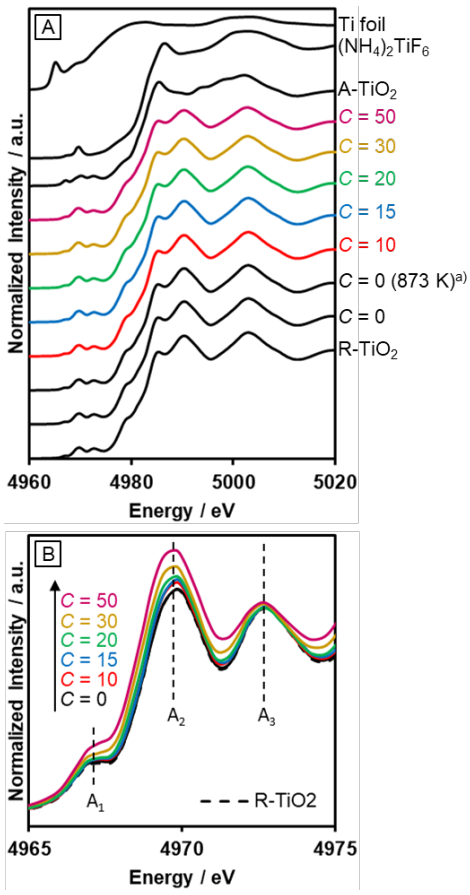

Fig. 5. Ti-K edge XANES of R-TiO_2:N,F obtained by nitriding the mixture of R-TiO_2 and $(NH_4)_2TiF_6$ with various concentration of $(NH_4)_2TiF_6$ at 773 K for 1 h. a) Nitrided at 873 K.

X-ray absorption spectroscopy

The incorporated nitrogen and fluorine into rutile TiO_2 also influenced the electronic state of Ti. Fig. 5A shows Ti-K edge XANES spectra of R-TiO_2:N,F. XANES spectra of R-TiO_2:N,F samples resemble that of rutile TiO_2, but different from Ti foil, $(NH_4)_2TiF_6$ and anatase TiO_2. This indicates that the local structure around Ti atoms in rutile TiO_2 remains largely unchanged even after nitrogen/fluorine doping. However, a distinct change was observed in three pre-edge peaks (Fig. 5B); A_1, A_2 and A_3 result from the hybridization of p and d orbitals of the local Ti absorber and surrounding neighbors.[55] The Ti 3d orbital of R-TiO_2:N,F, which has a TiA_6 (A = anion) octahedral unit, is split into the t_{2g} and e_g by a ligand field. The A_1 peak arises from the quadrupole transition of 1s to t_{2g} of the local Ti absorber. The A_2 peak is overlapped by two components, the quadrupole transition of 1s to e_g of the local Ti absorber and the dipole transition of 1s to t_{2g} of the neighboring Ti atoms. The A_3 peak is attributed to the dipole transition of 1s to e_g of the neighboring Ti atoms. Among the three pre-edge peaks, there is an obvious increase in the A_2 peak with increasing C values. In the displacive-type ferroelectricity of Ti oxides,[56] and in the nano-size effect of TiO_2,[57] it has been reported that the A_2 peak is increased by the local symmetry breaking around Ti atom, because the Ti d/p mixing induced by the distortion of the TiA_6 unit affects the quadrupole transition of 1s to e_g in the

A_2 peak. Therefore, the observed increase in the A_2 peak arise from the local distortion around Ti site caused by nitrogen/fluorine doping. We also measured N-K edge XANES spectra (Fig. S3). The result showed that irrespective of the *C* value, the nitrogen dopant in R-TiO_2:N,F existed in the form of lattice N^{3-}, somewhat similar to nitrogen-doped anatase TiO_2 that exhibits relatively high activity.[58]

On the basis of structural characterization using XRD, elemental analyses, SEM/EDX, STEM and XAFS, it is reasonably concluded that the prepared samples are nitrogen/fluorine-codoped rutile TiO_2, although the samples with higher *C* values tended to contain undesirable byproducts such as $TiOF_2$.

Optical properties and band-edge positions of rutile R-TiO_2:N,F

UV-visible diffuse reflectance spectra of the R-TiO_2:N,F samples are displayed in Fig. 6. Samples prepared using $(NH_4)_2TiF_6$ ($C \geq 10$) showed clear absorption in the visible region, in addition to intrinsic band-gap absorption of rutile TiO_2 at around 400 nm. By contrast, synthesis without $(NH_4)_2TiF_6$ did not produce a material that shows such distinct visible light absorption, even though the temperature for the synthesis was increased to 873 K. The visible light absorption was more pronounced with increasing the *C* value. It has been reported that the increase in the nitrogen content enhances visible light absorption in nitrogen-doped oxide materials.[16] Therefore, the more pronounced visible light absorption in the present R-TiO_2:N,F samples is attributed to increased nitrogen content, which is consistent with the result of elemental analysis (Table 1). It is noted that the absorption edge of R-TiO_2:N,F is located at longer wavelengths than that reported for anatase R-TiO_2:N,F.[17] The absorption at longer wavelengths (λ > 600 nm) is usually assigned to reduced titanium species.[17,18,59] A plausible reason for increase of reduced titanium species in samples synthesized with higher $(NH_4)_2TiF_6$ concentration is the reduction of TiO_2 by $(NH_4)_2TiF_6$.[16]

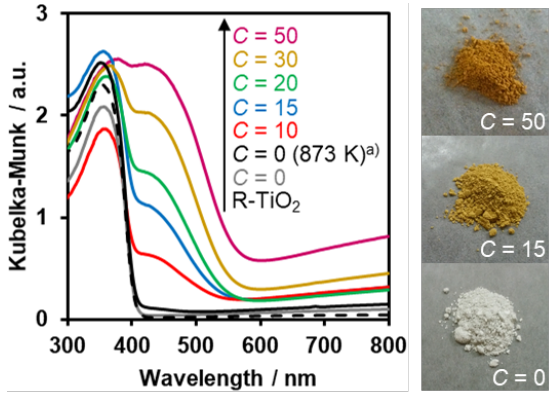

Fig. 6. DRS of R-TiO_2:N,F obtained by nitriding the mixture of R-TiO_2 and $(NH_4)_2TiF_6$ with various concentration of $(NH_4)_2TiF_6$ at 773 K for 1 h. a) Nitrided at 873 K.

In order to estimate the band potentials of R-TiO_2:N,F, electrochemical impedance measurements were conducted for *C* = 15 sample. As shown in Fig. S4, Mott-Schottky plots had a positive slope corresponding to n-type band bending. Flat band potentials estimated from these plots were –0.41 V, –0.72 V and –0.93 V vs. Ag/AgCl at pH 4.3, 6.7 and 9.8, respectively. These values correspond to 0.03 V, –0.13 V, –0.15 V vs. RHE, which is close to the reported value for rutile TiO_2 at 0 V (vs. RHE).[60] Of course, we confirmed that the R-TiO_2:N,F sample is stable in the potential range examined (Fig. S5).

The conduction band edge potential of n-type semiconductors depends on their conductivity and locates at 0.1–0.3 V negative of the flat band potential.[60] In this study, the difference between conduction band potential and the flat band potential was assumed to be 0.2 V, since the conductivity of the material is not clear. Based on this assumption and the band gap determined from DRS, the band potentials were determined as shown in Fig. 7. The valence band edge of R-TiO_2:N,F is located at ca. 2.0 V vs. RHE, which is positive enough for water oxidation. This is 1.0 V above the reported rutile TiO_2 valence band, which is located at 3.0 V vs. RHE.

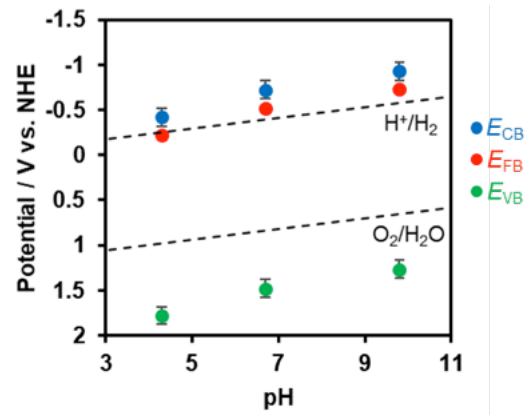

Fig. 7. Dependence of conduction and valence band edge potentials for R-TiO_2:N,F (*C* = 15) on pH of electrolyte, as determined from Mott-Schottky plots (see Fig. S4).

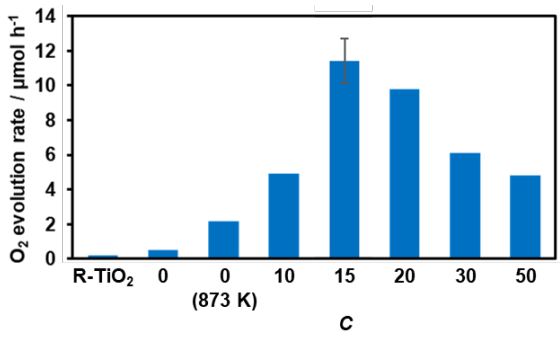

Fig. 8. Photocatalytic activity of R-TiO_2:N,F with different *C* values for O_2 evolution under visible light irradiation in $AgNO_3$ aqueous solution. Reaction conditions: catalyst, 50 mg; La_2O_3 200 mg; 10 mM $AgNO_3$ aqueous solution, 140 mL; light source, 300 W Xe lamp fitted with CM-1 mirror and L42 cutoff filter (λ > 420 nm). Average rate of O_2 evolution for the first 30 minutes of irradiation. Full time course data is shown in Fig. S6.

Photocatalytic water oxidation

Water oxidation activity was first examined using $AgNO_3$ as a sacrificial electron acceptor, in order to optimize the *C* value. As shown in Fig. 8, all of the synthesized materials produced O_2 upon visible light irradiation. However, the activities of the R-TiO_2:N,F samples differed with respect to *C* value. The photocatalytic activity of R-TiO_2:N,F increased abruptly as

increase in *C*, reaching maximum at *C* = 15, and then decreased gradually.

The O_2 evolution rate decreased with increasing the cutoff wavelength of the incident light (Fig. S7), indicating that the reaction occurred through light absorption by R-TiO_2:N,F. It is noteworthy that the present R-TiO_2:N,F was capable of producing O_2 even under >580 nm irradiation, different from anatase-type TiO_2:N,F that had shorter absorption edge than the rutile counterpart and did not work under the irradiation condition.[17]

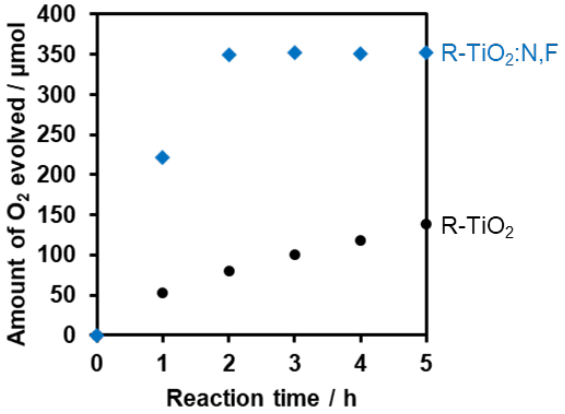

Fig. 9. Time courses of O_2 evolution on R-TiO_2 and R-TiO_2:N,F (*C* = 15) under UV irradiation in $AgNO_3$ aqueous solution. Reaction conditions: catalyst, 50 mg; La_2O_3 200 mg; 10 mM $AgNO_3$ aqueous solution, 140 mL; light source, 300 W Xe lamp fitted with CM-1 mirror (λ > 350 nm). The total amount of evolved O_2 (ca. 0.35 mmol) is one-fourth of that of Ag^+ (1.4 mmol), which is in reasonable agreement with the expected stoichiometry of the reaction; i.e., four-electron oxidation of water into O_2 and one-electron reduction of Ag^+.

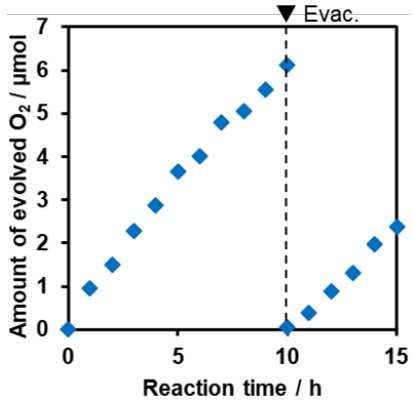

Fig. 10. Time course of O_2 evolution during photocatalytic reaction of RuO_2/R-TiO_2:N,F (C = 15) under visible light irradiation in $NaIO_3$ aqueous solution. Reaction conditions: catalyst, 50 mg; 10 mM $NaIO_3$ aqueous solution, 140 mL; light source, 300 W Xe lamp fitted with CM-1 mirror and L42 cutoff filter (λ > 420 nm).

It should be noted that the most active R-TiO_2:N,F (*C* = 15) showed higher rate of O_2 evolution than undoped rutile TiO_2 did even under >350 nm irradiation, where rutile TiO_2 is able to undergo photoexcitation (Fig. 9). In most cases, the photocatalytic activities of doped TiO_2 materials for water oxidation under UV irradiation are much lower than that of undoped one, despite the fact that the doped materials have superior light absorption capability (i.e., visible light absorption).[62–64] Therefore, the photocatalytic property of the present R-TiO_2:N,F appears unusual, and such property has scarcely been reported in visible-light-responsive doped TiO_2 materials for water oxidation. Apparent quantum yield of O_2 evolution on the R-TiO_2:N,F (*C* = 15) photocatalyst was measured to be ca. 6.4% at 365 nm, which was higher than that of R-TiO_2 (ca. 5.4%).[65]

Furthermore, it was found that the optimized R-TiO_2:N,F (*C* = 15) produced O_2 from aqueous solutions containing a reversible electron acceptor ($NaIO_3$), with the aid of a RuO_2 cocatalyst (Fig. 10). The water oxidation reaction with $NaIO_3$ is "non-sacrificial", as the change in Gibbs energy during the reaction is positive.[9] SEM observations indicated that the loaded RuO_2 on the R-TiO_2:N,F was in the form of nanoparticles of 10–20 nm in size (Fig. S8), which can work as both reduction and oxidation sites.[48] While the rate of O_2 evolution decreased slightly at the initial stage of the reaction (<5 h), it became constant after 5 h, as shown in Fig. 10. No noticeable change in XRD pattern and DRS could be identified before and after the 15 h of reaction (Fig. S9). O_2 evolution was also observed when Fe^{3+} was used as an electron acceptor (Fig. S10). These results indicate that the R-TiO_2:N,F works as a stable photocatalyst for water oxidation into O_2 under visible light even in the presence of a reversible electron acceptor.

Z-scheme water splitting

Finally, we applied the optimized R-TiO_2:N,F modified with a RuO_2 cocatalyst as the component of water oxidation in a Z-scheme water splitting system, in combination with a known H_2 evolution photocatalyst of Ru/$SrTiO_3$:Rh.[51] XRD pattern and UV-visible diffuse reflectance spectrum of the as-prepared $SrTiO_3$:Rh are shown in Fig. S11. We employed a $[Co(bpy)_3]^{3+/2+}$ couple as a shuttle redox mediator, which can mediate electron transfer from a suitable O_2 evolution photocatalyst to the H_2 evolution Ru/$SrTiO_3$:Rh photocatalyst.[51] In the Z-scheme system, forward reactions that occur on the Ru/$SrTiO_3$:Rh surface are as follows:

$$2H^+ + 2e^- \rightarrow H_2 \quad (1)$$

$$[Co(bpy)_3]^{2+} + h^+ \rightarrow [Co(bpy)_3]^{3+} \quad (2)$$

On the other hand, the forward reactions on an O_2 evolution photocatalyst are as follows:

$$[Co(bpy)_3]^{3+} + e^- \rightarrow [Co(bpy)_3]^{2+} \quad (3)$$

$$4OH^- + 4h^+ \rightarrow O_2 + 2H_2O \quad (4)$$

Fig. 11 shows that visible light irradiation of an aqueous $[Co(bpy)_3]^{2+}$ solution suspended with Ru/$SrTiO_3$:Rh and RuO_2/R-TiO_2:N,F resulted in stoichiometric H_2 and O_2 evolution without noticeable degradation even for 35 h of irradiation. Here the total amount of reacted electrons during the reaction (159 μmol [= 4 × evolved O_2], see Fig. 11) was much greater than that of $[Co(bpy)_3]^{2+}$ (60 μmol), indicating that the $[Co(bpy)_3]^{3+/2+}$ couple was cycled during the reaction. This system was also workable even under simulated sunlight irradiation (Fig. S12), giving a solar energy conversion efficiency of 0.02%.[66] No reaction took place in the dark. Without using $[Co(bpy)_3]^{2+}$, the rates of H_2 and O_2 evolution were very low (Fig. S13), an order of magnitude lower than

those recorded with $[Co(bpy)_3]^{2+}$ (Fig. 11). It indicates that the contribution of Z-scheme water splitting through inter-particle electron transfer[67] was very small under the present reaction condition. Note that without a suitable O_2 evolution photocatalyst, only H_2 evolution was observed.[51] Using RuO_2/R-TiO_2 instead of RuO_2/R-TiO_2:N,F, the O_2 evolution activity decreased significantly (Fig. S14). This is because RuO_2/R-TiO_2 cannot efficiently reduce $[Co(bpy)_3]^{3+}$ and oxidize water under visible light due to its large band gap (Fig. 6).

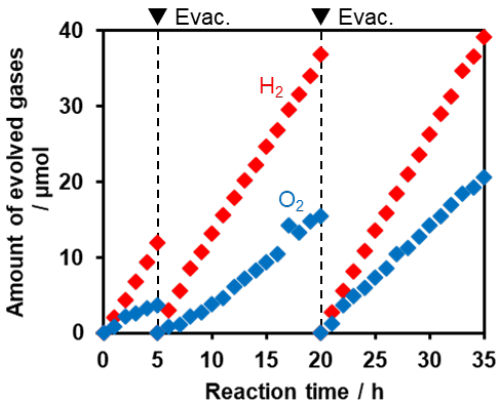

Fig. 11. Time course of H_2 and O_2 evolution from mixtures of RuO_2/R-TiO_2:N,F (C = 15) (50 mg) and Ru/$SrTiO_3$:Rh (25 mg) dispersed in an aqueous solution (120 mL) containing tris(2,2'-bipyridyl)cobalt(II) sulfate (0.5 mM) under visible-light irradiation (λ > 420 nm).

On the basis of these results, we concluded that Z-scheme overall water splitting into H_2 and O_2 is achieved using a mixture of Ru/$SrTiO_3$:Rh and RuO_2/R-TiO_2:N,F in the presence of $[Co(bpy)_3]^{3+/2+}$ as a shuttle redox mediator, and that RuO_2/R-TiO_2:N,F achieved the functionality as an O_2 evolution photocatalyst similar to oxide-based semiconductor photocatalysts (e.g., $BiVO_4$).[51] This is the first example of achieving visible-light-driven Z-scheme overall water splitting using a ternary mixed anion compound as the component of water oxidation.

Although H_2 and O_2 are simultaneously evolved from the same suspension in Z-scheme water splitting systems, Kudo et al. proposed a method to separately produce H_2 and O_2.[51] They developed a two-compartment reactor, in which H_2 and O_2 evolution photocatalysts are separately suspended in each compartment divided by a membrane filter that is permeable to a redox mediator.

Time-resolved visible to mid-infrared absorption spectroscopy

To further understand the effect of nitrogen/fluorine codoping on the energy levels in the band gap, time-resolved visible to mid-infrared absorption spectroscopy measurements were conducted. As shown in Fig. 12, the shape of the transient absorption spectra depended on dopants as well as their concentration. This suggests that trap states in the band gap of rutile TiO_2 are altered by the anion doping. R-TiO_2:N,F (C = 0 (873 K)) shows absorption at around 7000 cm^{-1}, which is attributable to deeply trapped electrons.[24,41,42] Since oxygen vacancies have been reported as the most probable trap states in TiO_2,[68] the trap states can be ascribed to the oxygen vacancies caused by nitrogen doping. The absorption at around 7000 cm^{-1} tended to decrease upon fluorine codoping (i.e., with increasing C) up to C = 15. This strongly suggests that the density of the oxygen vacancies is reduced as the result of maintaining the charge balance (i.e. $2O^{2-} \leftrightarrow N^{3-} + F^-$). In addition, an absorption at around 18000 cm^{-1} increased sharply, which is assigned to trapped holes.[44,45] Importantly, the existence of the signal from trapped holes suggests that the sample has reactive holes that can be used for water oxidation reactions.[44,45] While the trapped hole signal was more pronounced upon further increase in C from 15 to 50, an absorption centred at around 5000 cm^{-1} increased. This suggests that new trap states were formed in samples with larger C values. It is also noted that a signal observed at 3000–1000 cm^{-1}, which is due to shallowly trapped and/or free electrons,[40,42] disappeared with increasing the C value from 15 to 50. This means that the lifetime of mobile electrons in R-TiO_2:N,F was shortened upon excess increase in fluorine codoping.

Factors affecting the water oxidation activity of rutile R-TiO_2:N,F

The result of photocatalytic reactions indicated that the water oxidation activity of R-TiO_2:N,F depended on the C value in the synthesis. The increased activity with increasing C is most likely due to the difference in visible-light absorption. That is, more visible light absorption leads to an increase in the number of available photons to the water oxidation reaction. However, this could not account for the decrease in activity at higher C values.

The time-resolved visible to mid-IR absorption

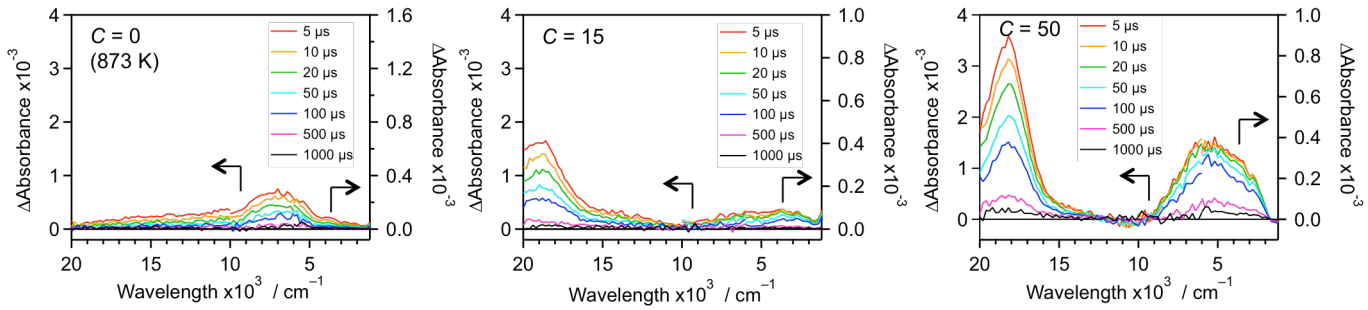

Fig. 12. Transient absorption spectra for R-TiO_2:N,F with different C values excited with 480 nm laser pulses under N_2 atmosphere. Transmittance and reflectance were measured below and above 6000 cm^{-1}, respectively. Data for the C = 10 and 30 samples are shown in Fig. S15.

measurements revealed that there is a difference in carrier dynamics of the R-TiO_2:N,F with different *C* values. *C* = 15 sample, which showed highest water oxidation activity, has relatively low density of mid-gap states, compared to samples with smaller and larger *C* values. This feature would be responsible for the high photocatalytic activity of *C* = 15 sample, in addition to the improved light absorption capability. The reason for the activity drop from *C* = 15 to 50 can be explained by the emergence of mid-gap states that deeply trap photogenerated charge carriers. Since deeply trapped carriers are usually less reactive,[41,69,70] this is most likely the main cause of the decrease in the photocatalytic activity for larger *C* values. Thus, it can be concluded that enhancement of light absorption while suppressing the formation of trap states for photogenerated carriers is important for the high photocatalytic activity.

Conclusions

Nitrogen/fluorine-codoped rutile TiO_2 (R-TiO_2:N,F) was successfully synthesized by nitriding a mixture of rutile TiO_2 and $(NH_4)_2TiF_6$. R-TiO_2:N,F exhibited higher photocatalytic activity under visible light irradiation than only nitrogen-doped analogue did. R-TiO_2:N,F was also applicable to non-sacrificial water oxidation using IO_3^- or Fe^{3+} as a reversible electron acceptor when modified with a RuO_2 cocatalyst. The RuO_2-loaded R-TiO_2:N,F was found to work as an O_2 evolution photocatalyst for visible-light-driven Z-scheme water splitting, in combination with Ru/$SrTiO_3$:Rh H_2 evolution photocatalyst and a $[Co(bpy)_3]^{3+/2+}$ shuttle redox mediator. Physicochemical analyses indicated that the key to achieve high water oxidation activity of the R-TiO_2:N,F photocatalyst is appropriate adjustment of N/F codoping level, which maximizes visible light absorption while minimizing the density of deep trap states in the band gap structure of R-TiO_2:N,F.

Recently, the codoping strategy with N^{3-} and F^- has been applied to non-TiO_2 photocatalysts for tuning the band gap as well as exploring a new crystal phase.[71–73] Although photocatalytic activities of such ternary mixed-anion compounds have been reported, no strategy to improve the photocatalytic activity based on photogenerated charge carrier dynamics had been established. Therefore, we believe that the results of the present study shed light on the development of N/O/F-based ternary compounds, which exhibit high photocatalytic activity under visible light.

Conflicts of interest

There are no conflicts to declare.

Acknowledgements

This work was supported by a Grant-in-Aid for Scientific Research on Innovative Area "Mixed Anion (Project JP16H06438, JP16H06440, JP16H06441 and JP17H05491)" (JSPS). It was also partially supported by Grant-in-Aids for Young Scientists (A) (Project JP16H06130) and for Challenging Research (Exploratory) (Project JP17K19169). K.M. acknowledges the Noguchi Institute, The Hosokawa Powder Technology Foundation and the PRESTO/JST program "Chemical Conversion of Light Energy" for financial support. S.Nishioka acknowledges financial support from Grant-in-Aid for JSPS Fellows from JSPS. The authors also would like to express gratitude to Profs. Tsutomu Minegishi and Kazunari Domen (The University of Tokyo) for assistance with electrochemical impedance measurements.

Author contributions

A.M. and K.M. designed the project and wrote a draft of the manuscript. A.M. conducted most of the experiments and analyses. J.J.M.V. and A.Y. performed transient absorption spectroscopy with A.M. S.Nishioka synthesized $SrTiO_3$:Rh and modified it with a Ru cocatalyst. Y.K., M.Y., S.Nozawa and T.Y. performed XAFS measurement with A.M. S.Y. and K.K. conducted STEM observation. A.I. and A.K. synthesized the cobalt complex. All of the authors discussed and provided comments on the experiments and the manuscript during preparation.

Notes & References

1 H. Kageyama, K. Hayashi, K. Maeda, J. P. Attfield, Z. Hiroi, J. M. Rondinelli and K. R. Poeppelmeier, *Nat. Commun.,* 2018, **9**, 772.
2 W. J. Youngblood, S.-H. A. Lee, K. Maeda and T. E. Mallouk, *Acc. Chem. Res.,* 2009, **42**, 1966.
3 A. Kudo and Y. Miseki, *Chem. Soc. Rev.*, 2009, **38**, 253.
4 K. Maeda, *J. Photochem. Photobiol., C*, 2011, **12**, 237.
5 R. Abe, *Bull. Chem. Soc. Jpn.,* 2011, **84**, 1000.
6 Y. Wang, X. Wang and M. Antonietti, *Angew. Chem., Int. Ed.*, 2012, **51**, 68.
7 F. E. Osterloh, *Chem. Soc. Rev.*, 2013, **42**, 2294.
8 Y. Ma, X. Wang, Y. Jia, X. Chen, H. Han and C. Li, *Chem. Rev.*, 2014, **114**, 9987.
9 K. Maeda and K. Domen, *Bull. Chem. Soc. Jpn.,* 2016, **89**, 627.
10 K. Takanabe, *ACS Catal.*, 2017, **7**, 8006.
11 S. Sato, T. Arai and T. Morikawa, *Inorg. Chem.*, 2015, **54**, 5105.
12 R. Kuriki and K. Maeda, *Phys. Chem. Chem. Phys.*, 2017, **19**, 4938.
13 K. Maeda, *Progress in Solid State Chem.*, 2018, in press. DOI: 10.1016/j.progsolidstchem.2017.11.003.
14 R. Asahi, T. Morikawa, T. Ohwaki, K. Aoki and Y. Taga, *Science*, 2001, **293**, 269.
15 T. Morikawa, R. Asahi, T. Ohwaki, K. Aoki and Y. Taga, *Jpn. J. Appl. Phys.*, 2001, **40**, L561.
16 K. Nukumizu, J. Nunoshige, T. Takata, J. N. Kondo, M. Hara, H. Kobayashi and K. Domen, *Chem. Lett.*, 2003, **32**, 196.
17 K. Maeda, Y. Shimodaira, B. Lee, K. Teramura, D. Lu, H. Kobayashi and K. Domen, *J. Phys. Chem. C*, 2007, **111**, 18264.
18 K. Maeda, B. Lee, D. Lu and K. Domen, *Chem. Mater.*, 2009, **21**, 2286.
19 D. Li, H. Haneda, S. Hishita and N. Ohashi, *Chem. Mater.*, 2005, **17**, 2588.
20 X. Zong, Z. Xing, H. Yu, Z. Chen, F. Tang, J. Zou, G. Q. Lu and L. Wang, *Chem. Commun.*, 2011, **47**, 11742.
21 N. Kumar, U. Maitra, V. I. Hegde, U. V. Waghmare, A. Sundaresan and C. N. R. Rao, *Inorg. Chem.*, 2013, **52**, 10512.

22 H. Liu and L. Gao, *J. Am. Ceram. Soc.*, 2004, **87**, 1582.
23 S. Yin, K. Ihara, Y. Aita, M. Komatsu and T. Sato, *J. Photochem. Photobiol., A*, 2006, **179**, 105.
24 A. Nakada, S. Nishioka, J. J. M. Vequizo, K. Muraoka, T. Kanazawa, A. Yamakata, S. Nozawa, H. Kumagai, S. Adachi, O. Ishitani and K. Maeda, *J. Mater. Chem. A*, 2017, **5**, 11710.
25 R. Abe, K. Sayama and H. Sugihara, *J. Phys. Chem. B*, 2005, **109**, 16052.
26 O.-O. Prieto-Mahaney, N. Murakami, R. Abe and B. Ohtani, *Chem. Lett.,* 2009, **38**, 238.
27 T. Ohno, D. Haga, K. Fujihara, K. Kaizaki and M. Matsumura, *J. Phys. Chem. B*, 1997, **101**, 6415.
28 K. Maeda, *Chem. Commun.*, 2013, **49**, 8404.
29 K. Maeda, N. Murakami and T. Ohno, *J. Phys. Chem. C*, 2014, **118**, 9093.
30 R. Li, Y. Weng, X. Zhou, X. Wang, Y. Mi, R. Chong, H. Han and C. Li, *Energy Environ. Sci.*, 2015, **8**, 2377.
31 K. Maeda, M. Higashi, D. Lu, R. Abe and K. Domen, *J. Am. Chem. Soc.*, 2010, **132**, 5858.
32 K. Maeda, D. Lu and K. Domen, *ACS Catal.*, 2013, **3**, 1026.
33 W. Zhao, K. Maeda, F. Zhang, T. Hisatomi and K. Domen, *Phys. Chem. Chem. Phys.*, 2014, **16**, 12051.
34 K. Iwashina, A. Iwase, Y. H. Ng, R. Amal and A. Kudo, *J. Am. Chem. Soc.*, 2015, **137**, 604.
35 D. A. H. Hanaor and C. C. Sorrell, *J. Mater. Sci.*, 2011, 46, 855.
36 J. C. Yu, J. Yu, W. Ho, Z. Jiang and L. Zhang, *Chem. Mater.*, 2002, **14**, 3808.
37 H. Chen, A. Nambu, W. Wen, J. Graciani, Z. Zhong, J. C. Hanson, E. Fujita and J. A. Rodriguez, *J. Phys. Chem. C*, 2007, **111**, 1366.
38 A. Yamakata, T.-a. Ishibashi and H. Onishi, *J. Phys. Chem. B*, 2001, **105**, 7258.
39 A. Yamakata, M. Yoshida, J. Kubota, M. Osawa and K. Domen, *J. Am. Chem. Soc.*, 2011, **133**, 11351.
40 K. Furuhashi, Q. Jia, A. Kudo and H. Onishi, *J. Phys. Chem. C*, 2013, **117**, 19101.
41 A. Yamakata, H. Yeilin, M. Kawaguchi, T. Hisatomi, J. Kubota, Y. Sakata and K. Domen, *J. Photochem. Photobiol., A*, 2015, **313**, 168.
42 A. Yamakata, J. J. M. Vequizo and H. Matsunaga, *J. Phys. Chem. C*, 2015, **119**, 24538.
43 F. Zhang, A. Yamakata, K. Maeda, Y. Moriya, T. Takata, J. Kubota, K. Teshima, S. Oishi and K. Domen, *J. Am. Chem. Soc.*, 2012, **134**, 8348.
44 M. Hojamberdiev, K. Yubuta, J. J. M. Vequizo, A. Yamakata, S. Oishi, K. Domen and K. Teshima, *Cryst. Growth Des.*, 2015, **15**, 4663.
45 M. Hojamberdiev, H. Wagata, K. Yubuta, K. Kawashima, J. J. M. Vequizo, A. Yamakata, S. Oishi, K. Domen and K. Teshima, *Appl. Catal. B: Environ.*, 2016, **182**, 626.
46 H. Zhang, Y. Chen, R. Lu, R. Li and A. Yu, *Phys. Chem. Chem. Phys*., 2016, **18**, 14904.
47 R. Godin, Y. Wang, M. A. Zwijnenburg, J. Tang and J. R. Durrant, *J. Am. Chem. Soc*., 2017, **139**, 5216.
48 K. Maeda, R. Abe and K. Domen, *J. Phys. Chem. C*, 2011, **115**, 3057.
49 H. Suzuki, S. Nitta, O. Tomita, M. Higashi and R. Abe, *ACS Catal.*, 2017, **7**, 4336.
50 B. Ravel and M. Newville, *J. Synchrotron Rad.,* 2005, **12**, 537.
51 Y. Sasaki. H, Kato and A. Kudo, *J. Am. Chem. Soc.*, 2013, **135**, 5441.
52 K. Kimoto, T. Asaka, X. Yu, T. Nagai, Y. Matsui and K. Ishizuka, *Ultramicroscopy*, 2010, **110,** 778.
53 S. D. Findlay, N. Shibata, H. Sawada, E. Okunishi, Y. Kondo and Y. Ikuhara, *Ultramicroscopy*, 2010, **110**, 903.
54 S. J. Pennycook and D. E. Jesson, *Ultramicroscopy*, 1991, **37**, 14.
55 T. Uozumi, A. Kotani and J. C. Parlebas, *J. Electron Spectrosc. Relat. Phenom.*, 2004, **137–140**, 623.
56 S. Nozawa, T. Iwazumi, H. Osawa and T. Uozumi, *Appl. Phys. Express*, 2013, **6***,* 061501.
57 L. X. Chen, T. Rajh, Z. Wang and M. C. Thurnauer, *J. Phys. Chem. B,* 1997, **101**, 10688.
58 T. Yoshida, S. Niimi, M. Yamamoto, T. Nomoto and S. Yagi, *J. Colloid Interface Sci.*, 2015, **447**, 278.
59 A. Kasahara, K. Nukumizu, G. Hitoki, T. Takata, J. N. Kondo, M. Hara, H. Kobayashi and K. Domen, *J. Phys. Chem. A,* 2002, **106**, 6750.
60 L. Kavan, M. Grätzel, S. E. Gilbert, C. Klemenz and H. J. Scheel, *J. Am. Chem. Soc.,* 1996, **118**, 6716.
61 Matsumoto, Y. *J. Solid State Chem*. **1996**, *126*, 227
62 H. Kato and A. Kudo, *J. Phys. Chem. B,* 2002, **106**, 5029.
63 R. Niishiro, H. Kato and A. Kudo, *Phys. Chem. Chem. Phys.,* 2005, **7**, 2241.
64 R. Niishiro, R. Konta, H. Kato, W.-J. Chun, K. Asakura and A. Kudo, *J. Phys. Chem. C,* 2007, **111**, 17420.
65 The apparent quantum yield (AQY) for the water oxidation reaction was measured using the same experimental setup, except for the addition of a band-pass filter (λ = 365 nm) and output current (10 A), and was estimated according to the equation (AQY (%) = (A × R/I) × 100), where A, R and I represent coefficients based on the reaction (O_2 evolution, 4), the O_2 evolution rate and the rate of incident photons, respectively. The total number of incident photons (ca. 0.88 mW) was measured using a calibrated silicon photodiode.
66 Solar energy conversion efficiency (η) was calculated according to the following equation: η (%) = $R_H \cdot \Delta G^0$ / ($P \cdot S$) × 100. Here R_H, ΔG^0, P, and S indicate the rate of hydrogen evolution (mol s^{-1}) in Z-scheme water splitting, standard Gibbs energy of water (237.13 × 10^3 J mol^{-1}), the intensity of simulated sunlight (100 mW cm^{-2}) from a solar simulator (Asahi Spectra, HAL-320) and irradiation area (16 cm^2), respectively. The irradiance of the solar simulator almost (ca. 95%) corresponds to that of AM1.5G.
67 Y. Sasaki, H. Nemoto, K. Saito and A. Kudo, *J. Phys. Chem. C*, 2009, **113**, 17536.
68 S. Ikeda, N. Sugiyama, S. Murakami, H. Kominami, Y. Kera, H. Noguchi, K. Uosaki, T. Torimoto and B. Ohtani, *Phys. Chem. Chem. Phys.*, 2003, **5**, 778.
69 R. Kuriki, H. Matsunaga, T. Nakashima, K. Wada, A. Yamakata, O. Ishitani and K. Maeda, *J. Am. Chem. Soc.*, 2016, **138**, 5159.
70 K. Wada, C. S. K. Ranasinghe, R. Kuriki, A. Yamakata, O. Ishitani and K. Maeda, *ACS Appl. Mater. Interfaces*, 2017, **9**, 23869.
71 N. Kumar, J. Pan, N. Aysha, U. V. Waghmare, A. Sundaresan and C. N. R. Rao, *J. Phys. Condens. Matter*, 2013, **25**, 345901.
72 S. Yoon, A. E. Maegli, L. Karvonen, S. K. Matam, A. Shkabko, S. Riegg, T. Großmann, S. G. Ebbinghaus, S. Pokrant and A. Weidenkaff, *J. Solid State Chem.*, 2013, **206**, 226.
73 S. R. Lingampalli, K. Manjunath, S. Shenoy, U. V. Waghmare and C. N. R. Rao, *J. Am. Chem. Soc.*, 2016, **138**, 8228.

TOC entries

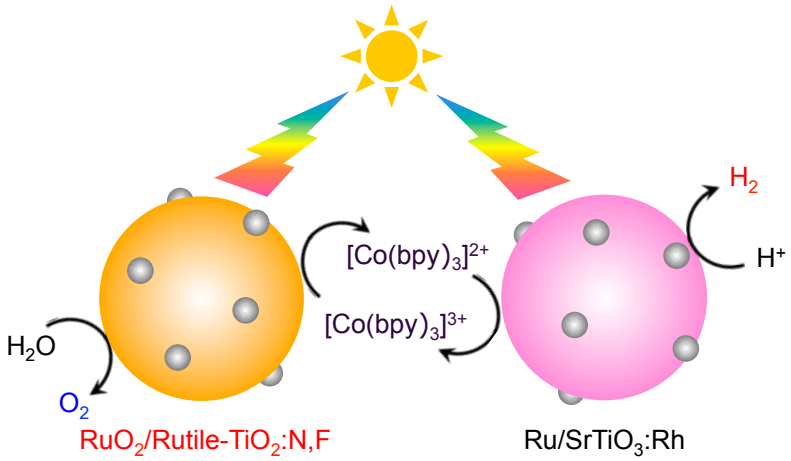

We developed nitrogen/fluorine-codoped rutile TiO_2 as a water oxidation photocatalyst for solar-driven Z-scheme water splitting.